UDC 541.136+546.33+544.463+541.138

DOI: 10.15372/CSD2021311

Perspective Cathode Materials for Sodium-Ion Batteries

N. V. KOSOVA, D. O. SEMYKINA

Institute of Solid State Chemistry and Mechanochemistry, Siberian Branch of the Russian Academy of Sciences, Novosibirsk, Russia

E-mail: kosova@solid.nsc.ru

(Received February 16, 2021; revised March 23, 2021)

Abstract

Sodium-ion batteries (SIBs) are the nearest alternative to lithium-ion batteries (LIBs) for stationary energy storage devices. However, at the moment, SIBs are inferior to LIBs in energy density due to the lower efficiency of sodium-containing electrode materials, which encourages the emergence of new developments in this field. The review provides examples of some promising sodium-containing cathode materials obtained by mechanochemically assisted solid-state synthesis. It is shown that this approach is an energy- and eco-efficient method for the synthesis of single-phase, nanostructured cathode materials. An increase in their electron conductivity is achieved through surface modification with an electronically conductive carbon at the stage of synthesis. A complex of modern physicochemical methods was used to study their crystal and local structure, morphology, and electrochemical properties during cycling in both Na and Li electrochemical cells. The specific energy was compared with that of the known lithium-containing cathode materials.

Keywords: sodium-ion batteries, sodium-containing cathode materials, mechanical activation

INTRODUCTION

During recent years, an urgent issue is a problem concerning the replacement of lithium-ion electrochemical systems, which are widely used at present, by sodium-ion ones. This replacement will eliminate the problems of lithium deficiency on the Earth and the high cost of lithium-containing materials. The most promising application of sodium-ion rechargeable batteries (SIBs) is large-scale energy storage systems, so the availability of raw material and its low cost, high operation resource and fire safety retain decisive importance [1–4]. Physicochemical characteristics of sodium are similar to those of lithium, however, sodium is more widespread in nature, and its cost is much lower. At the same time, SIBs are distinguished by a lower efficiency of electrode materials and energy density than those of lithium-ion rechargeable batteries (LIBs) because the oxidation-reduction potential of the Na^+/Na couple (−2.71 V vs. the standard hydrogen electrode) is higher by 0.3 V than the potential of the Li^+/Li couple, while the molar mass is larger.

One of the major elements of a rechargeable battery, determining its characteristics, is the material of positive electrodes (cathodes). Polyanion compounds are considered a promising class of cathode materials for SIBs. The compounds of this class possess mainly framework structure, due to which a small change in unit cell volume is observed during reversible (de)intercalation of sodium ions. This improves their structural stability during cycling and, as a consequence, increases their operation lifetime, while a strong covalent bond of oxygen with a nonmetal within the anion ensures the absence of O_2 evolution, thus enhancing their performance safety.

Initially, the search for electrode materials for SIBs was carried out relying on the principle of analogy with the known lithium cathode materi-

TABLE 1
Characteristics of lithium polyanion cathode materials in comparison with sodium derivatives

Li-derivative	S. G.	U_m, V	Q, (mA · h)/g	Synthesis method	Reference	Na-derivative	S. G.	U, V	Q, mA · h/g	Synthesis method	Reference
$LiFePO_4$ (olivine)	*Pnma*	3.4	169	SS	[5]	$NaFePO_4$ (maricite)	*Pnmb*	–	–	SS	[12]
						*$NaFePO_4$ (olivine)	*Pnma*	2.9	154	Li/Na exchange	[13]
$Li_2FeP_2O_7$	$P2_1$	3.5	110	SS	[6]	$Na_2FeP_2O_7$	*P*-1	3.0	90	SS	[14]
$LiFePO_4F$	*P*-1	3.0	152	SS	[7]	Na_2FePO_4F	*Pnmb*	3.0	124	SS	[12]
*Li_2FePO_4F	*P*-1	3.0	152	E/C							
$Li_9Fe_3(PO_4)_2(P_2O_7)_3$	*P*-3*c*	2.75	85	Sol-gel	[8]	$Na_4Fe_3(PO_4)_2P_2O_7$	$Pn2_1a$	2.9/3.2	127	SS	[15]
$Li_9V_3(PO_4)_2(P_2O_7)_3$	*P*-3*c*	3.8/4.5	174	SS	[9]	$Na_7V_4PO_4(P_2O_7)_4$	$P\text{-}42_1c$	3.9	93	SS	[16]
$LiVPO_4F$	*P*-1	4.1	156	SS	[10]	$NaVPO_4F$	$C2/c$ $P4_2/mnm$	–	–	Quenching	[17]
						$Na_3V_2(PO_4)_2F_3$		3.9	128	SS	[18]
$Li_3V_2(PO_4)_3$	$P2_1/n$	3.6/3.7/4.1/4.4	133	SS	[11]	$Na_3V_2(PO_4)_3$	*R*-3	3.4	118	SS	[19]

Note. SS – solid-state, HT – hydrothermal, E/C – electrochemical intercalation.
* The compound cannot be obtained through direct synthesis.

als. However, it became clear soon that they differ in composition, structure and electrochemical characteristics. Comparative characteristics of lithium and sodium cathode materials similar to each other in composition are listed in Table 1. One can see that there are differences in structure and in working voltage for the same compounds of lithium and sodium [5–19]. For instance, $NaFePO_4$, which is analogous to $LiFePO_4$ with olivine structure, a widespread cathode material for LIBs, may be obtained directly only in the form of maricite, in which there are no channels for the diffusion of sodium ions and thus no electrochemical activity is observed [12]. $NaFePO_4$ with olivine structure is usually obtained from $LiFePO_4$ through chemical Li/Na ion exchange [13]. Tavorite-like vanadium(III)-lithium fluoro-phosphate $LiVPO_4F$ is a promising cathode material for LIBs [10], however, its sodium derivative, vanadium(III)-sodium fluoro-phosphate $NaVPO_4F$, is metastable (may be obtained only under non-equilibrium conditions) and does not exhibit electrochemical activity [17]. On the other hand, fluoro-phosphate with a different structure, $Na_3V_2(PO_4)_2F_3$, is obtained through direct solid-phase synthesis; it is considered at present as one of the cathode materials for SIBs most close to commercialization [18].

Sodium-containing cathode materials, which are synthesized in an easier manner than lithium-containing ones, as a rule, may be considered as matrices for reversible intercalation of Li^+ ions. In addition, mixed Li/Na-materials may in some cases possess different, more stable crystal structures with larger diffusion channels due to the presence of larger Na^+ ions, which promotes acceleration of (de)intercalation process and hence leads to the improvement of power characteristics. These materials are obtained using two procedures: either sodium-containing cathode materials are subjected to preliminary electrochemical removal of sodium, and their subsequent cycling is performed in a Li-cell, or initially mixed Li/Na-compounds are synthesized, for example using the solid-state route.

In the present review, some examples of promising sodium-containing cathode materials obtained by mechanochemically assisted solid-state synthesis are described. Their crystal and local structure, morphology and electrochemical characteristics during cycling both in Na- and in Li-electrochemical cells were studied by means of a set of modern physicochemical methods.

EXPERIMENTAL

Cathode materials were synthesized using the mechanochemically assisted solid-state method. Preliminary mechanical activation (MA) was carried out in a high-energy planetary mill AGO-2 (900 min^{-1}) in stainless steel cylinders with steel balls. The mass ratio of powder to balls was 1 : 40. Mechanically activated mixtures were annealed in argon flow.

X-ray diffraction analysis (XRD) of the samples was carried out with a D8 Advance diffractometer (Bruker, Germany) with CuK_α-radiation (l_1 = 1.5406 Å, l_2 = 1.5445 Å). GSAS and TOPAS software packages were used to refine the structures according to XRD data. The size and morphology of particles were studied by means of scanning electron microscopy (SEM) and transmission electron microscopy (TEM) using a scanning electron microscope S3400N (Hitachi, Japan) and a transmission electron microscope JEM-220FS (JEOL, Japan) with the resolution of 0.1 nm. Mössbauer spectra were recorded with an NP 255/610 spectrometer (Hungary) with Co^{57} γ-radiation at room temperature, and infrared (IR) spectra were recorded with a Tensor 27 instrument (Bruker, Germany) within the range 200–4000 cm^{-1}. Thermal analysis (DTA) was carried out using an STA 449 F/1/1JUPITER thermoanalyzer (Netzsch, Germany), chemical analysis was performed by means of energy-dispersive X-ray spectroscopy (EDS) using an UltraDry EDS detector.

For electrochemical tests, cathode masses composed of the active component (75 mass %), conducting carbon Super P (20 mass %), and PVDF/NMP binder (5 mass %) were prepared. The working electrodes were prepared by depositing the slurry on aluminium foil and drying at 100 °C in vacuum. The density of thus prepared samples was 2–3 mg/cm, electrode diameter was 10 mm. Sodium or lithium foil was used as the anode, and a 1 M $NaPF_6$ ($LiPF_6$) solution in a mixture of ethylene carbonate and propylene carbonate/dimethyl carbonate (1 : 1) was used as the electrolyte. Glass fibre filter Grade GF/C, Whatman was used as a separator. Electrochemical cells were mounted in an argon glovebox. Samples were cycled in a Biologic BCS 805 set-up in the galvanostatic mode both in Na-, and in Li-electrochemical cells.

RESULTS AND DISCUSSION

Iron(II)-sodium fluoro-phosphate Na_2FePO_4

In 2007, fluoro-phosphates of *d*-metals and sodium Na_2MPO_4F (M = Fe, Mn, Co, Ni) were proposed as a new class of compounds for SIBs. From the theoretical point of view, these materials may recover up to two sodium ions with the participation of two electrons of the *d*-metal per one formula unit (for example, at increased temperature [20]), which should provide high theoretical specific discharge capacity (>240 (mA · h)/g). In addition, the structure of Na_2MPO_4F is characterized by a small change in the unit cell volume during charging-discharging, which has a positive effect on cathode stability during cycling as a consequence of the absence of mechanical strain. These materials possess two-dimensional – 2*D* (Na_2FePO_4F, Na_2CoPO_4F), and three-dimensional – 3*D* (Na_2MnPO_4F) channels for the transport of alkaline metal ions, which promotes intercalation-deintercalation at a high rate. A disadvantage of these materials is low electronic conductivity and ion diffusion [20]. The electrical conductivity of Na_2MPO_4F may be increased if these compounds are obtained in a nano-sized state or by making a highly conductive carbon coating and/or doping.

The most promising compound of the Na_2MPO_4F family is iron(II)-sodium fluoro-phosphate Na_2FePO_4F [12]. It is characterized by a orthorhombic structure with space group (S. G.) *Pbcn*, high operating voltage (3.0 V) and theoretical specific capacity (124 (mA · h)/g per 1 electron). The material is capable of cycling either in a cell with sodium anode and sodium electrolyte or in a cell with the lithium anode and lithium electrolyte.

In the present work, two-stage synthesis of Na_2FePO_4F was carried out according to reactions

$$Fe_2O_3 + C + 2NaHCO_3 + 2(NH_4)_2HPO_4 \rightarrow 2NaFePO_4 + 4NH_3 + 2CO_2 + CO + 4H_2O \quad (1)$$

$$NaFePO_4 + NaF \rightarrow Na_2FePO_4F \quad (2)$$

Reaction mixtures (1) and (2) were subjected to preliminary MA for 10 min, followed by annealing for 1 h at a temperature of 650 and 600 °C, respectively. So short MA promotes dispersing and fine mixing of the reagents sharply different in particle sizes (Fig. 1). In addition, the presence of carbon in the reaction mixture prevents the growth of product particles during subsequent annealing. According to SEM data, the final product Na_2FePO_4F is a nanostructured material with an average particle size of 200–300 nm (see Fig. 1).

According to XRD data, the product of reaction (1) is a single-phase $NaFePO_4$ with the maricite structure (S. G. *Pmnb*). Phase formation processes were studied by means of high-tem-

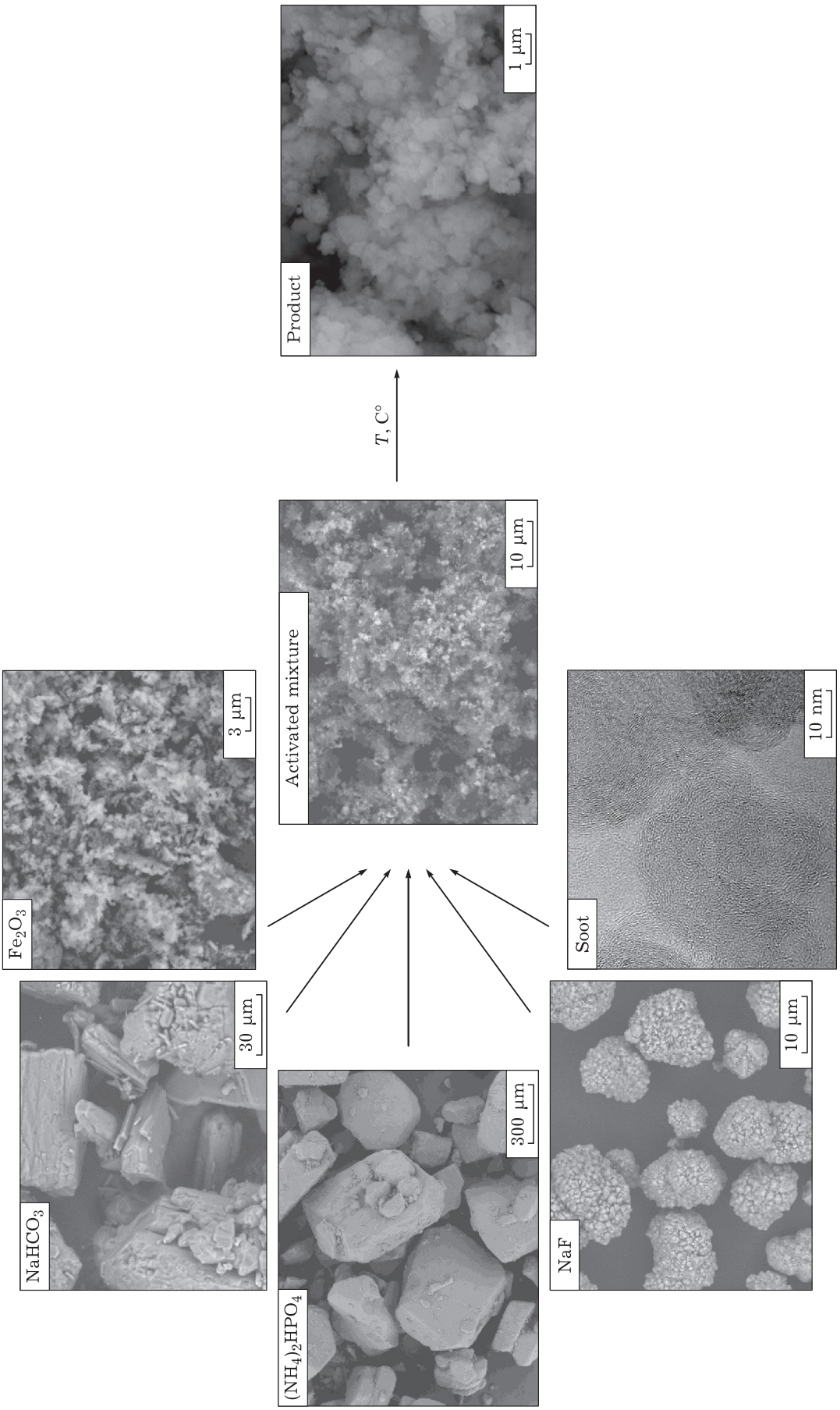

Fig. 1. SEM microphotographs of initial reagents, activated mixture and final product Na_2FePO_4F obtained as a result of subsequent annealing.

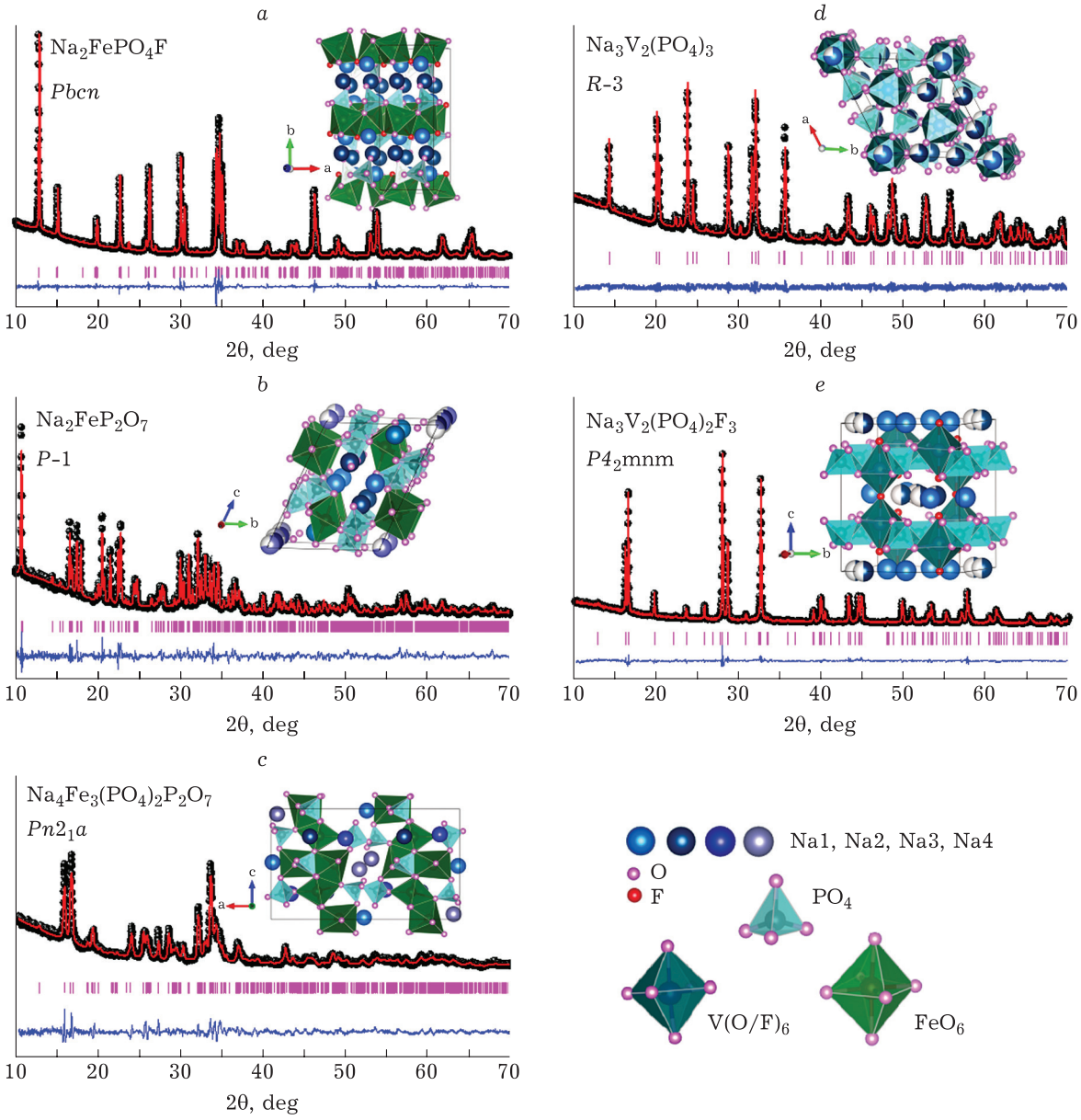

Fig. 2. Diffraction patterns of Na_2FePO_4F (*a*), $Na_2FeP_2O_7$ (*b*), $Na_4Fe_3(PO_4)_2P_2O_7$ (*c*), $Na_3V_2(PO_4)_3$ *d*) and $Na_3V_2(PO_4)_2F_3$ (*e*) after structural refinement according to the Rietveld method. Designations: black dots – experimental diffraction patterns; red and blue lines – calculated and differential curves, respectively; pink hatches – positions of the reflections from crystal phases. Inserts show the structures represented with the help of coordination polyhedrons marked in the legend to the right at the bottom.

perature XRD during heating the mixture (2) from 25 to 700 °C [12]. It was established that the intensity of reflections of the final product Na_2FePO_4F increases gradually with temperature rise to 500 °C, and then starts to decrease with further temperature rise. At 700 °C, the reflections of the Na_2FePO_4F phase disappear, and additional reflections appear, which is evidence of the decomposition of Na_2FePO_4F into Na_3PO_4, Fe_3O_4, $Na_{0.11}FeF_3$, $Na_3Fe_2(PO_4)_3$. To avoid product decomposition, subsequent synthesis was carried out at a temperature of 600 °C.

According to XRD data, the final product obtained after annealing in argon at 600 °C contains only one phase Na_2FePO_4F (Fig. 2, *a*). There are two crystallographic positions for sodium in the structure of Na_2FePO_4F: Na1 and Na2. The Na1 position is surrounded by four oxygen ions (Na–O distances are within the range of 2.30 to 2.47 Å) and two fluoride ions (Na–F distances are within the range of 2.29 to 2.48 Å). The Na2 position has four oxygen ligands with Na–O bonds varying in length from 2.19 to 2.59 Å, and two fluoride ligands at a distance of 2.34 and 2.36 Å from Na

ion. The Mössbauer spectra of Na_2FePO_4F are well described by one doublet, which points to the presence of Fe^{2+} ions in one octahedral position. The values of isomeric shift (IS) and quadrupole splitting (QS) are equal to 1.23 and 2.19 mm/s, respectively [12].

During Na_2FePO_4F cycling in the Na-cell, a two-step charge-discharge profile is observed at a voltage of 3.1 and 2.9 V; the discharge capacity is ~120 (mA · h)/g (Fig. 3). During cycling Na_2FePO_4F in the Li-cell within the voltage range of 2.0–4.2 V, the charge-discharge profile changes gradually within the first four cycles, which is the evidence of Na^+/Li^+ ion exchange. At the first charging step, Na^+ ions are extracted in two stages at the voltage of ~3.2 and ~3.5–3.6 V (Fig. 4). The discharge capacity of the sample without carbon coating is 55 (mA · h)/g and increases to 103 (mA · h)/g at the fourth cycle, while for the sample with carbon coating the capacity is equal to 81 and 116 (mA · g)/g, respectively (see Fig. 4). Starting from the fifth cycle, the capacity is stabilized, which is indirect evidence that the formation of the new phase is complete in the course of the electrochemical reaction. Indeed, according to XRD and EDS data, the composition of the phase formed in this process is close to $NaLiFePO_4F$ with S. G. *Pbcn*.

Investigation of the possibility to synthesize mixed compositions $Na_{2-x}Li_xFePO_4F$ ($0 \le x \le 1$) by means of mechanochemically assisted solid-state synthesis using $NaFePO_4$, $LiFePO_4$, NaF and LiF as the starting reagents was carried out. It was established that three individual compounds are formed in the Na_2FePO_4F–Li_2FePO_4F system: Na_2FePO_4F, $Na_{1.5}Li_{0.5}FePO_4F$ and $NaLiFePO_4F$, with the structures described by the S. G. *Pnma* with 1*D*-channels for the diffusion of alkaline metal ions. All mixed Na/Li-containing compounds obtained through solid-state synthesis are electrochemically active during cycling in the Li-cell. The specific discharge capacity of $NaLiFePO_4F$ is 115 (mA · h)/g with an average voltage of 3.3 V.

Iron-sodium pyrophosphates $Na_2FeP_2O_7$

Pyrophosphates of *d*-metals and sodium $Na_2MP_2O_7$ (M = Co, Mn, Ni, Mg) have been extensively studied by crystallographers during the two recent decades [6]. It was established that these compounds are crystallized mainly in triclinic symmetry with the space group *P*1 or *P*-1. Only in 2012 Yamada and co-authors [14] reported on the promising electrochemical properties of iron-sodium pyrophosphate $Na_2FeP_2O_7$ obtained by means of conventional solid-state synthesis at 600 °C, and the possibilities of its use as the cathode material for SIBs. The average operating voltage of $Na_2FeP_2O_7$ is 3 V with respect to Na/Na^+, and its theoretical capacity is 97 (mA · h)/g.

By varying the Na/Fe ratio in the system $Na_{2-x}Fe_{1+x/2}P_2O_7$, two compounds differing from each other in composition may be synthesized: with $x = 0$ and $x = 0.44$ [21, 22]. Both compounds have triclinic structures (sp. gr. *P*-1), but differ from each other by the number of Na positions. Six nonequivalent Na positions may be distinguished in $Na_2FeP_2O_7$, while there are only four positions in $Na_{1.56}Fe_{1.22}P_2O_7$. The structure of $Na_{1.56}Fe_{1.22}P_2O_7$ is more disordered. The FeO_6 octahedrons and P_2O_7-groups form tunnels in the directions [100], [-110] and [01-1], promoting easy and rapid migration of Na^+ ions (see Fig. 2, *b*). The formation of antisite defects is characteristic of $Na_2FeP_2O_7$; Na^+ and Fe^{2+} ions exchange their positions in these defects. However, since Na^+ ion (r = 1.02 Å) is substantially larger than Li^+ ion (r = 0.76 Å) and Fe^{2+} ion (r = 0.78 Å), antisite defects are less pronounced for $Na_2FeP_2O_7$ in comparison with its lithium analogue $Li_2FeP_2O_7$. The degree of disorder should be temperature-dependent and therefore sensitive to the experimental synthesis conditions. The three-dimensional nature of the paths of alkaline ion migration in $Na_2FeP_2O_7$ means that antisite defects much less hinder its transport properties, and this material should possess good power characteristics. Though iron-sodium pyrophosphates are characterized by the high sensitivity to air components, the surface oxidation of materials may vary depending on particle morphology and the thickness of the carbon layer.

In the present work, iron-sodium pyrophosphates $Na_2FeP_2O_7$ and $Na_{1.56}Fe_{1.22}P_2O_7$ were obtained by mechanochemically assisted solid-state synthesis using the stoichiometric mixtures of Na_2CO_3, $FeC_2O_4 \cdot 2H_2O$ and $(NH_4)_2HPO_4$ as reagents according to the equation:

$$(1 - x/2)Na_2CO_3 + (1 + x/2)FeC_2O_4 \cdot 2H_2O + 2(NH_4)_2HPO_4 \rightarrow Na_{2-x}Fe_{1+x/2}P_2O_7 + 4NH_3\uparrow + 2CO_2\uparrow + (1 + x/2)CO\uparrow + (5 + x)H_2O;\ (x = 0;\ 0.44) \quad (3)$$

To provide a conducting carbon coating, soot was added into reaction mixture in the amount of 3 mass % of the final product. Initial mixture was subjected to preliminary MA for 5 min and annealed at 600 °C for 2 h in Ar flow [21].

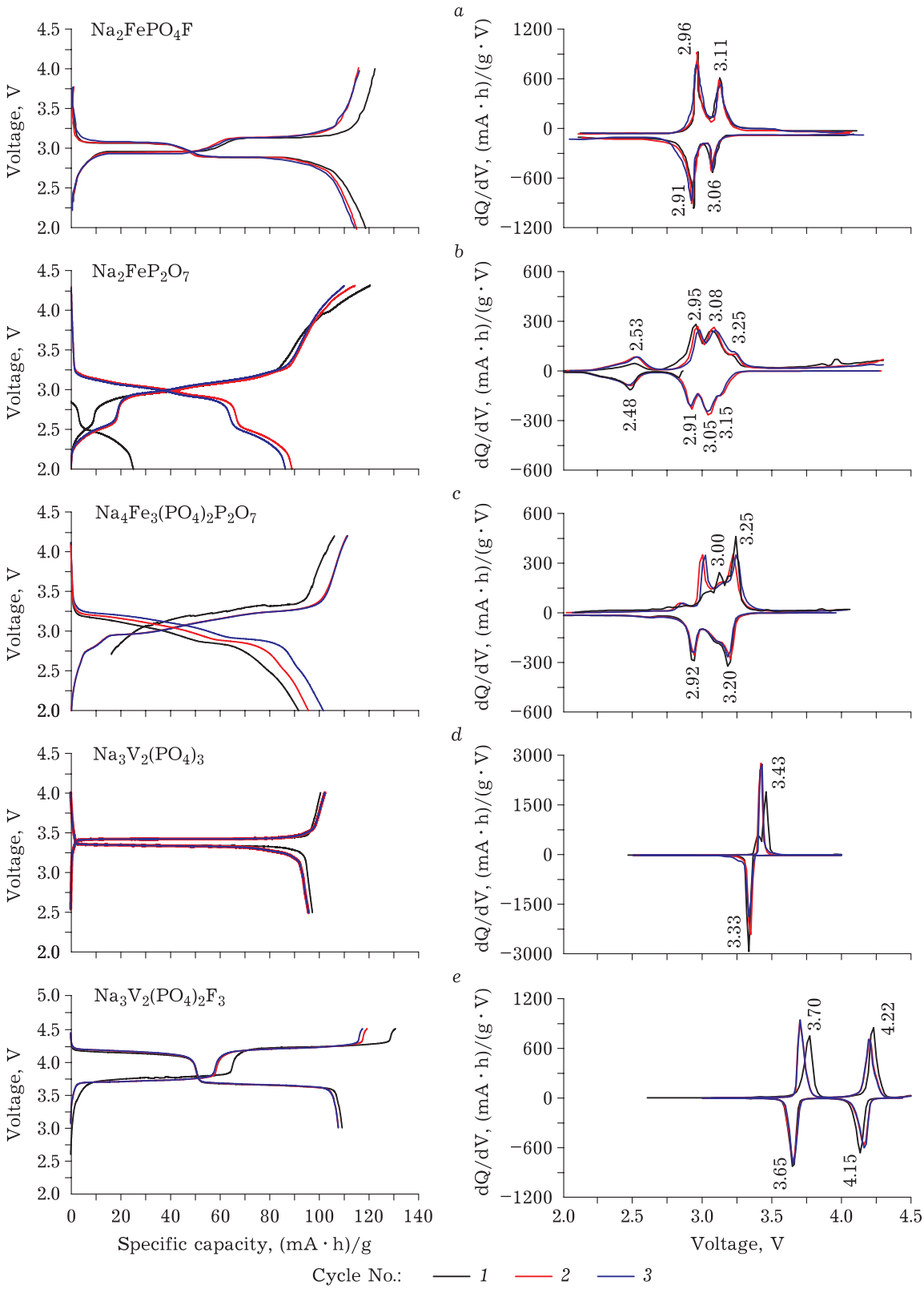

Fig. 3. Charge-discharge curves for Na_2FePO_4F (*a*), $Na_2FeP_2O_7$ (*b*), $Na_4Fe_3(PO_4)_2P_2O_7$ (*c*), $Na_3V_2(PO_4)_3$ (*d*) and $Na_3V_2(PO_4)_2F_3$ (*e*) in the Na-cells (vs. Na-anode) and the corresponding dependences of d*Q*/d*U* vs. voltage.

According to XRD data, the resulting $Na_2FeP_2O_7$ and $Na_{1.56}Fe_{1.22}P_2O_7$ samples are practically single-phase and possess triclinic structure (see Fig. 2, *b*). According to SEM data, the samples are composed

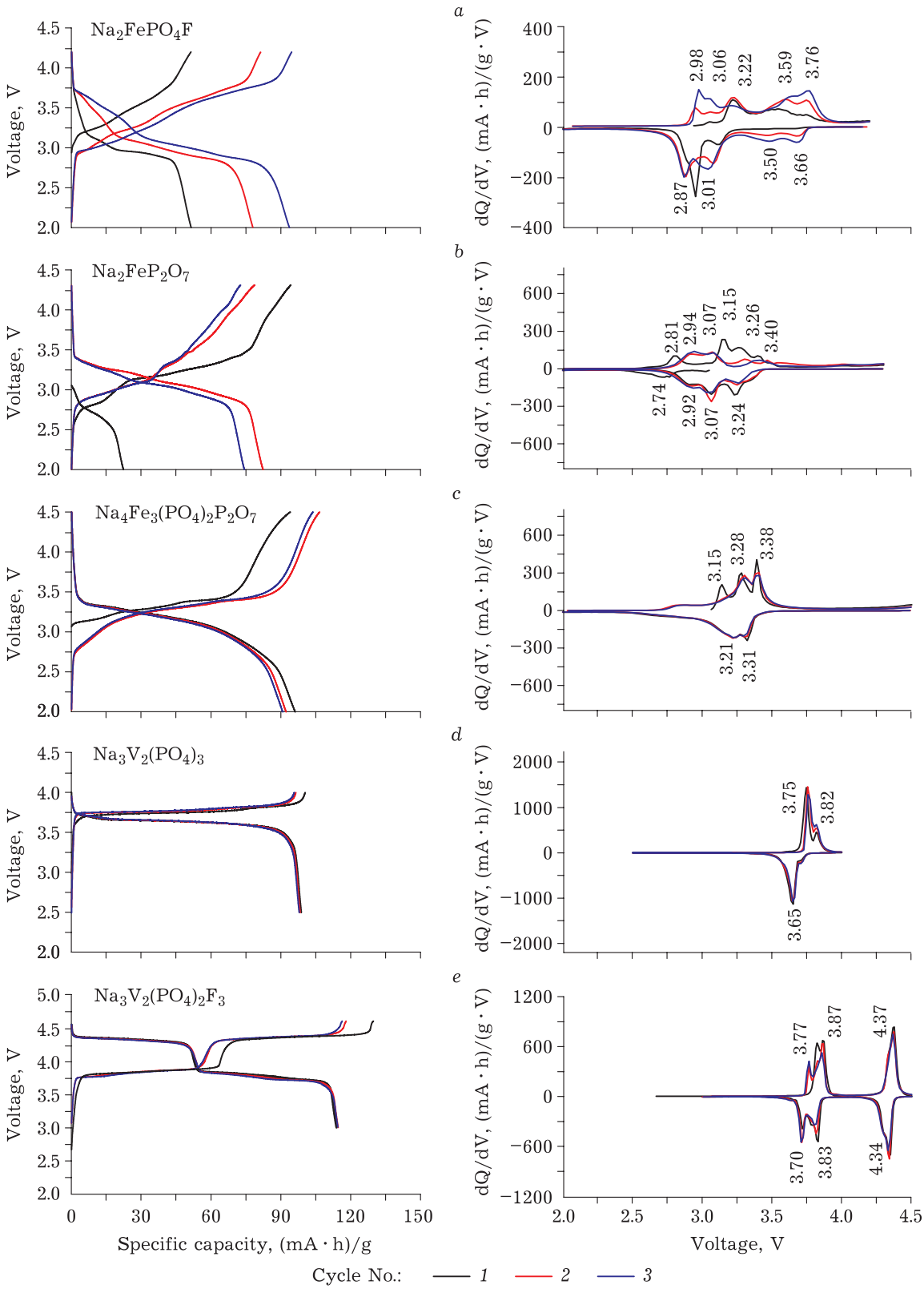

Fig. 4. Charge-discharge curves for Na_2FePO_4F (*a*), $Na_2FeP_2O_7$ (*b*), $Na_4Fe_3(PO_4)_2P_2O_7$ (*c*), $Na_3V_2(PO_4)_3$ (*d*) and $Na_3V_2(PO_4)_2F_3$ (*e*) in the Li-cells (vs. Li-anode) and the corresponding dependences vs. d*Q*/d*U* vs. voltage.

of a mixture of fine (primary) particles with an average size of 300–500 nm and larger secondary particles of micron size arising as a result of the agglomeration of the primary particles [21].

The IR spectra of the samples, in addition to the vibrations of pyrophosphate groups, contain an additional band at 1450 cm^{-1}, related to the vibrations of CO_3^{2-} group, which is the evidence of the surface instability of these materials to the atmospheric air [21]. The band is more intense in the case of $Na_2FeP_2O_7$ in comparison with $Na_{1.56}Fe_{1.22}P_2O_7$. The occurrence of sample interaction with air components is confirmed also by the data of Mössbauer spectroscopy [21]. In addition to two basic doublets related to the structural positions of Fe^{2+}, Mössbauer spectra contain also a doublet assigned to Fe^{3+} ions. In this situation, $Na_2FeP_2O_7$ contains about 23 % Fe^{3+}, while $Na_{1.56}Fe_{1.22}P_2O_7$ contains only 7 %, which is evidence of the higher stability of the latter compound to air. The oxidation of Fe^{2+} ions proceeds according to the reaction:

$$Na_2FeP_2O_7 + 1/2O_2 + xCO_2 \rightarrow Na_2CO_3 + Na_{2-2x}Fe^{2+}_{1-2x}Fe^{3+}_{2x}P_2O_7 \quad (4)$$

Cycling of $Na_2FeP_2O_7$ and $Na_{1.56}Fe_{1.22}P_2O_7$ was performed in Na-cells with Na-anode and Na-electrolyte, as well as in Li-cells with Li-anode and Li-electrolyte. The charge-discharge profiles of the first and the third cycles for $Na_2FeP_2O_7$ in Na-cell at a rate of $C/20$ (where C/n is current density at which the material should reach theoretical capacity C within n hours) within voltage range 2.0–4.3 V are shown in Fig. 3, *b*. Since the sample contained a substantial amount of Fe^{3+} ions, so cycling started from the discharging stage (pre-discharge), in order to reduce the existing Fe^{3+} ions to Fe^{2+}. The specific discharge capacity was 25 (mA · h)/g, which corresponds to the intercalation of 26 % additional Na^+ ions per formula unit and is in good agreement with the amount of Fe^{3+} determined by means of Mössbauer spectroscopy. Two regions are observed at the subsequent cycles: a small plateau at 2.5 V and a plateau at 3.0 V. On the contrary, $Na_{1.56}Fe_{1.22}P_2O_7$ demonstrates a sloping charge-discharge profile pointing to a single-phase reaction [21]. Specific discharge capacity at the pre-discharge stage is 13 (mA · h)/g. Though initial discharge capacity of $Na_{1.56}Fe_{1.22}P_2O_7$ (84 (mA · h)/g, which is 72 % of its theoretical capacity) is lower than that for $Na_2FeP_2O_7$ (89 (mA · h)/g, which is 92 % of theoretical capacity), further on, it demonstrates more stable cycling [21].

It was shown for the first time that these pyrophosphates exhibit high electrochemical activity also during cycling in Li-cells with an average operating voltage of 3.2 V and specific discharge capacity 90 (mA · h)/g (see Fig. 4). The presence of partial Na/Li exchange was established by means of *ex-situ* XRD and EDS. This exchange is over at the 4^{th}–5^{th} cycle and leads to the formation of mixed Na/Li-pyrophosphates having the composition $NaLiFeP_2O_7$ for $Na_2FeP_2O_7$ and $Na_{1.2}Li_{0.36}Fe_{1.22}P_2O_7$ for $Na_{1.56}Fe_{1.22}P_2O_7$, possessing triclinic structure [22].

Iron-sodium orthopyrophosphates

Other examples of promising sodium cathode materials are mixed orthopyrophosphates $Na_4M_3(PO_4)_2P_2O_7$ (M = Fe, Mn, Co, Ni) [23]. The potential of the oxidation-reduction couple M^{2+}/M^{3+} in this family increases as a sequence Fe (3.0 V) < Mn (3.5 V) < Co (4.3 V) < Ni (4.9 V). These materials demonstrate a small change in volume during cycling (2–7 %), which implies their long operation lifetime [23]. The most interesting compounds are Fe- and Mn-containing orthopyrophosphates due to the availability of Fe- and Mn-containing raw materials in the environment. Though $Na_4Mn_3(PO_4)_2P_2O_7$ has a higher working voltage than $Na_4Fe_3(PO_4)_2P_2O_7$, it demonstrates a more substantial degradation of capacity during cycling. Mixed iron-sodium orthopyrophosphate $Na_4Fe_3(PO_4)_2P_2O_7$ (NFPP) is characterized by the highest working voltage (3.1 V with respect to Na/Na^+) among sodium-iron containing cathode materials [24]: cathodes with olivine structure $NaFePO_4$ (2.7 V), amorphous iron phosphate $FePO_4$ (2.4 V), fluoro-phosphate Na_2FePO_4F and pyrophosphate $Na_2FeP_2O_7$. Large tunnels in the orthorhombic structure of NFPP provide paths for the diffusion of Na^+ ions with low activation barriers. Three of four Na^+ ions per formula unit participate in charge-discharge processes; the theoretical capacity of NFPP is equal to 127 (mA · h)/g.

NFPP crystallizes in the orthorhombic structure with S. G. $Pn2_1a$ [24]. The crystalline framework of NFPP is composed of a three-dimensional network of infinite layers $[Fe_3P_2O_{13}]\infty$, parallel to the *b*-*c* plane. The $[Fe_3P_2O_{13}]\infty$ layers are bound along the *a* axis by P_2O_7 groups, which makes large tunnels providing the diffusion of Na^+ ions.

NFPP was obtained by mechanochemically assisted solid-state synthesis. The reagents were stoichiometric amounts of $Na_4P_2O_7$, $Fe_2C_2O_4 \cdot 2H_2O$ and $(NH_4)_2HPO_4$ [15]. Soot was added to the reagent mixture in the amount of 3 mass % of the final product to make a carbon coating. The mixture was subjected to short-term (5 min) MA and

annealing at different temperatures from 400 to 600 °C for 4 h in Ar flow. The annealed mixtures were then cooled to room temperature with different rates (natural cooling in the furnace, or quenching).

It was established by means of XRD, IR and Mössbauer spectroscopy that NFPP prepared by annealing the activated mixture at 450 °C (NFPP-450) is the most pure-phase sample (see Fig. 2, *c*). At temperatures above 500 °C, NFPP decomposes due to thermal instability to form $NaFePO_4$ (maricite) and $Na_2FeP_2O_7$ [15]. For the quenched sample, the yield of the product reaches 94 mass %. So, NFPP with high phase homogenity may be obtained only within a narrow temperature range (400–500 °C). According to SEM data, NFPP-450 is composed of particles of submicron size, and according to TEM data, the average size of these particles is about 100 nm [15].

The NFPP-450 sample exhibits the best electrochemical properties during cycling both in Na- and in Li-cells among the samples obtained at other temperatures. The operating voltage in the Li-cell is higher by 0.2 V than in the Na-cell. It was determined that NFPP cycling in the Li-cell involves partial Na^+/Li^+ ion exchange, which leads to the formation of mixed Na/Li orthopyrophosphates (see Fig. 4). It was established that Li^+ ions are unstable in the structure of $Na_{4-x}Li_xFe_3(PO_4)_2P_2O_7$ (NLFPP), while the remaining Na^+ ions, quite contrary, stabilize the structure of NLFPP during cycling, in particular at a high rate. The joint (de) intercalation of Na^+ and Li^+ ions occurs during cycling in the Li-cell at the side of the cathode. The mixed NLFPP compositions may be considered as promising cathode materials for the batteries with high energy and power characteristics and as ion sieves to separate Na^+ and Li^+ ions.

Vanadium(III)-sodium phosphates and fluoro-phosphates

Vanadium-sodium phosphate $Na_3V_2(PO_4)_3$ belongs to NASICON-like compounds and possesses high ionic conductivity. $Na_3V_2(PO_4)_3$ is crystallized in the trigonal system with S. G. *R*-3 and possessed a stable three-dimensional framework. The latter is formed by $V_2(PO_4)_3$ structural units, which are composed of PO_4 tetrahedrons connected through their vertices with VO_6 octahedrons. The average working voltage of $Na_3V_2(PO_4)_3$ is 3.4 V vs. Na/Na^+, and theoretical specific capacity is 118 (mA · h)/g. Reversible intercalation of Na^+ ions is accompanied by minimal structural changes [19].

Replacement of one phosphate ion PO_4^{3-} in $Na_3V_2(PO_4)_3$ by F^- ion results in the formation of vanadium-sodium fluoro-phosphate $Na_3V_2(PO_4)_2F_3$, so the average operating voltage of the cathode material increases to 3.9 V [25–27]. $Na_3V_2(PO_4)_2F_3$ is the final representative of the family of mixed-valence vanadium-sodium fluoro-phosphates $Na_3V_2O_{2x}(PO_4)_2F_{3-2x}$ in which the degree of vanadium ion oxidation varies from 3+ ($x = 0$) to 4+ ($x = 1$). $Na_3V_2(PO_4)_2F_3$ (NVPF) is crystallized in the tetragonal system with S. G. $P4_2/mnm$ and has a stable three-dimensional framework formed by the structural units $V_2F_3(PO_4)_2$, composed of PO_4 tetrahedrons bound through their vertices to bioctahedrons $V_2F_3O_8$ [25]. NVPF is characterized by the presence of 2*D*-diffusion channels in the directions [110] and [1-10]. The average operating voltage is 3.9 V. Theoretical specific capacity is equal to 128 (mA · h)/g.

In this work, $Na_3V_2(PO_4)_3$ and $Na_3V_2(PO_4)_2F_3$ were synthesized using the solid-state method with preliminary MA [18]. $Na_3V_2(PO_4)_3$ was obtained in one stage from the stoichiometric mixture of Na_2CO_3, $(NH_4)_2HPO_4$, (V_2O_5 + C), while $Na_3V_2(PO_4)_2F_3$ was synthesized in two stages with preliminary synthesis of VPO_4 as precursor according to reactions

$$3Na_2CO_3 + 2V_2O_5 + 6(NH_4)_2HPO_4 + 2C \rightarrow 2Na_3V_2(PO_4)_3 + 12NH_3 + 4CO + 3CO_2 + 9H_2O \quad (5)$$

$$V_2O_5 + 2(NH_4)_2HPO_4 + 2C \rightarrow 2VPO_4 + 4NH_3\uparrow + 2CO\uparrow + 3H_2O\uparrow \quad (6)$$

$$2VPO_4 + 3NaF \rightarrow Na_3V_2(PO_4)_2F_3 \quad (7)$$

The diffraction patterns of the samples with structure refined using the Rietveld method point to the formation of single-phase products with the corresponding structure (see Fig. 2, *d*, *e*). It was established that the synthesis of $Na_3V_2(PO_4)_2F_3$ with decreased NaF/VPO_4 ratio leads to the products in which admixture phases are present in addition to the major phase [18]. The compound having the composition $NaVPO_4F$ is formed after solid-state synthesis only when quenching is applied [17].

During galvanostatic cycling of $Na_3V_2(PO_4)_3$ in Na- and Li-cells, one plateau is observed on charge-discharge curves at 3.4 and 3.7 V, respectively, corresponding to one intense oxidation-reduction peak (see Fig. 3, *d* and 4, *d*). Specific discharge capacity in the Na-cell is equal to 100 (mA · h)/g, and in the Li-cell it is ~98 (mA · h)/g. As the results of EDS and *ex-situ* XRD show, the

degree of electrochemical Na/Li ion exchange during $Na_3V_2(PO_4)_3$ cycling in the Li cell is 66 %, which corresponds to the formation of the compound with the composition $Li_2NaV_2(PO_4)_3$.

The average operating voltage at $Na_3V_2(PO_4)_2F_3$ cycling in the Na cell is 3.9 V, and the initial discharge capacity is equal to 115 (mA · h)/g (see Fig. 3, *e*). Two plateaus are observed on charge-discharge curves at 3.7 and 4.2 V, and the differential curves exhibit three redox peaks. Two poorly separated low-voltage peaks correspond to (de)intercalation of Na^+ ions from partially occupied Na2 positions in the structure of $Na_3V_2(PO_4)_2F_3$, while the third peak relates to (de)intercalation of Na^+ ions from completely occupied Na1 positions. During cycling in Li cells, the average operating voltage is 4.05 V, and the specific discharge capacity is 116 (mA · h)/g. This is accompanied by partial Na/Li-ion exchange, which is completed after the 4^{th}–5^{th} cycle. The degree of electrochemical Na/Li ion exchange is ~20 %, which corresponds to the formation of the compound with the composition $Na_{2.4}Li_{0.6}V_2(PO_4)_2F_3$. The structure of the formed mixed Na/Li fluorophosphates remains unchanged [22]. Later on, mixed (de)intercalation of Na^+ and Li^+ ions occurs on the cathode. The samples are well cycling also at increased rates.

The phase composition of mixed Na/Li fluorophosphates depending on the conditions of solid-state synthesis was studied. It was shown that the region of the formation of solid solutions is much narrower in this case than during electrochemical ion exchange, which is likely to be connected with the absence of structural similarity between the final compounds $Na_3V_2(PO_4)_2F_3$ and $LiVPO_4F$: $Na_3V_2(PO_4)_2F_3$ has a trigonal structure with S. G. $P4_2/mnm$ [18], while $LiVPO_4F$ is crystallized in the triclinic system with S. G. P-1 [10]. It was established that solid-state synthesis may be accompanied by the formation of V_2O_3 admixture with high electronic conductivity, which promotes an increase in sample conductivity by four orders of magnitude in comparison with initial $Na_3V_2(PO_4)_2F_3$ and improved cycling at increased rates both in Na-and in Li-cells [28]. The reason for increased capacity at increased cycling rate is partially due to the effect of pseudo-capacity initiated by the rational design of the material, in particular submicron particle size and *in situ* formed mixed coating composed of electroconducting carbon and V_2O_3.

The cation substitution of V^{3+} ions (r = 0.640 Å) in $Na_3V_2(PO_4)_2F_3$ by the ions of trivalent metals Al^{3+} (r = 0.535 Å), Fe^{3+} (r = 0.645 Å) and La^{3+} (r = 1.032 Å) was studied. It was determined that solid solutions are formed in the system within the studied Al^{3+} and Fe^{3+}, concentration range (2–7 at. %), while in the case of La^{3+} vanadium is not substituted by lanthanum because of a substantial difference in the ion radii of La^{3+} and V^{3+}. Instead, admixture phase $LaPO_4$ is formed; its particles are statistically distributed among $Na_3V_2(PO_4)_2F_3$ particles. The formation of $LaPO_4$ leads to an increase in the NaF/VPO_4 ratio in the reaction mixture and to the formation of sodium-containing surface admixture phase Na_3VF_6 with the high electronic conductivity, which finally provides high power characteristics of the obtained material [29].

Specific energy values for the studied sodium-containing cathode materials during cycling in Na- and Li-cells in comparison with the known lithium-containing cathode materials are presented in Fig. 5. One can see that $Na_3V_2(PO_4)_2F_3$ is the most efficient material among the studied ones.

CONCLUSION

Sodium-containing cathode materials Na_2FePO_4F, $Na_2Fe_2P_2O_7$, $Na_4Fe_3(PO_4)_2P_2O_7$, $Na_3V_2(PO_4)_3$, $Na_3V_2(PO_4)_2F_3$ with the high values of operating voltage vs. Na/Na^+ and high specific discharge capacity are promising for use in SIBs. It is demonstrated that mechanochemically assisted solid-state synthesis may be used successfully to obtain these compounds in a nanostructured state with surface modification by conducting carbon and with suitable electrochemical characteristics. These compounds may be considered as the matrices for reversible intercalation of Li^+ ions and hence as cathode materials for LIBs.

The production of SIBs requires the same fabrication lines as those for LIBs. This allows one to minimize primary investment, to provide high technological value, and thus defines the commercial attractiveness of SIBs.

Acknowledgements

The work was carried out within Project No. FWUS-2021-0006.

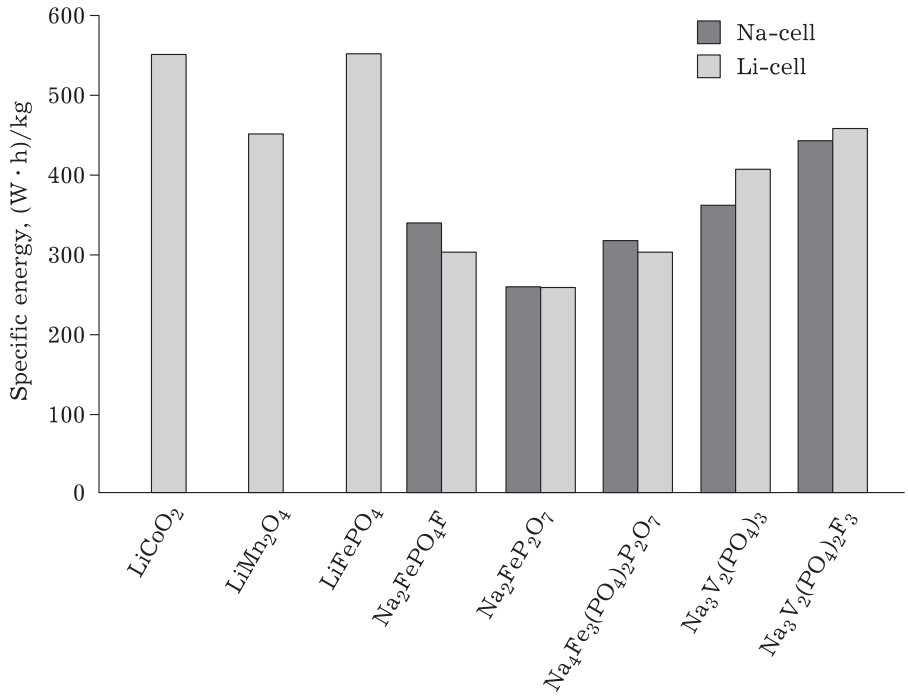

Fig. 5. Comparison between specific energies of sodium- and lithium-containing cathode materials.

REFERENCES

1 Yabuuchi N., Kubota K., Dahbi M., Komaba S., Research development on sodium-ion batteries, *Chem. Rev.*, 2014, Vol. 114, P. 11636–11683.

2 Dai Z., Mani U., Tan H. T., Yan Q., Advanced cathode materials for sodium-ion batteries: What determines our choices? *Small Methods*, 2017, No. 1700098.

3 Wang T., Su D., Shanmukaraj D., Rojo T., Armand M., Wang G., Electrode materials for sodiumion batteries: Considerations on crystal structures and sodium storage mechanisms, *Electrochem. Energy Reviews*, 2018, Vol. 1, P. 200–237.

4 Hwang J.-Y., Myung S.-T., Sun Y.-K., Sodium-ion batteries: Present and future, *Chem. Soc. Rev.*, 2017, Vol. 46, No. 12, P. 3529–3614.

5 Padhi A. K., Nanjundaswamy K. S., Masquelier C., Okada S., Goodenough J. B., Effect of structure on the Fe^{3+}/Fe^{2+} redox couple in iron phosphates, *J. Electrochem. Soc.*, 1997, Vol. 144, P. 1609–1613.

6 Nishimura S., Nakamura M., Natsui R., Yamada A., New lithium iron pyrophosphate as 3.5 V class cathode material for lithium ion battery, *J. Am. Chem. Soc.*, 2010, Vol. 132, No. 39, P. 13596–13597.

7 Ramesh T. N., Lee K. T., Ellis B. L., Nazar L. F., Tavorite lithium iron fluorophosphate cathode materials: Phase transition and electrochemistry of $LiFePO_4F$–Li_2FePO_4F, *Electrochem. Solid-State Lett.*, 2010, Vol. 13, P. A43–A47.

8 Gao H., Zhang S., Deng C., The first investigation of the synthetic mechanism and lithium intercalation chemistry of $Li_9Fe_3(P_2O_7)_3(PO_4)_2$/C as cathode material for lithium ion batteries, *Dalton Trans.*, 2015, Vol. 44, P. 138–145.

9 Kuang Q., Xu J., Zhao Y., Chen X., Chen L., Layered monodiphosphate $Li_9V_3(P_2O_7)_3(PO_4)_2$: A novel cathode material for lithium-ion batteries, *Electrochim. Acta*, 2011, Vol. 56, No. 5, P. 2201–2205.

10 Gover R. K. B., Burns P., Bryan A., Saidi M. Y., Swoyer J. L., Barker J., $LiVPO_4F$: A new active material for safe lithium-ion batteries, *Solid State Ionics*, 2006, Vol. 177, P. 2635–2638.

11 Morcrette M., Leriche J.-B., Patoux S., Wurm C., Masquelier C., In situ X-Ray diffraction during lithium extraction from rhombohedral and monoclinic $Li_3V_2(PO_4)_3$, *Electrochem. Solid-State Lett.*, 2003, Vol. 6, No. 5, P. A80–A84.

12 Kosova N. V., Podugolnikov V. R., Devyatkina E. T., Slobodyuk A. B., Structure and electrochemistry of $NaFePO_4$ and Na_2FePO_4F cathode materials prepared *via* mechanochemical route, *Mater. Research Bull.*, 2014, Vol. 60, P. 849–857.

13 Oh S. M., Myung S. T., Hassoun J., Scrosati B., Sun Y.-K., Reversible $NaFePO_4$ electrode for sodium secondary batteries, *Electrochem. Commun.*, 2012, Vol. 22, No. 1, P. 149–152.

14 Barpanda P., Liu G., Ling C. D., Tamaru M., Avdeev M., Chung S. C., Yamada Y., Yamada A., $Na_2FeP_2O_7$: A safe cathode for rechargeable sodium-ion batteries, *Chem. Mater.*, 2013, Vol. 25, No. 17, P. 3480–3487.

15 Kosova N. V., Belotserkovsky V. A., Sodium and mixed sodium/lithium iron *ortho*-pyrophosphates: Synthesis, structure and electrochemical properties, *Electrochim. Acta*, 2018, Vol. 278, P. 182–195.

16 Lim S. Y., Kim H., Chung J., Lee J. H., Kim B. G., Choi J.-J., Chung K. Y., Cho W., Kim S.-J., Goddard W. A. III, Jung Y., Choi J. W., Role of intermediate phase for stable cycling of $Na_7V_4(P_2O_7)_4PO_4$ in sodium ion battery, *PNAS*, 2014, Vol. 111, No. 2, P. 599–604.

17 Semykina D. O., Yakovlev I. V., Lapina O. B., Kabanov A. A., Kosova N. V., Crystal structure and migration paths of alkaline ions in $NaVPO_4F$, *Phys. Chem. Chem. Phys.*, 2020, Vol. 22, P. 15876–15884.

18 Kosova N. V., Semykina D. O., Mechanochemically assisted solid-state synthesis of sodium vanadium fluorophosphates, *Solid State Ionics*, 2019, Vol. 343, No. 115119.

19 Jian Z., Zhao L., Pan H., Hu Y.-S., Li H., Chen W., Chen L., Carbon coated $Na_3V_2(PO_4)_3$ as novel electrode material for sodium ion batteries, *Electrochem. Comm.*, 2012, Vol. 14, No. 1, P. 86–89.

20 Ellis B. L., Makahnouk W. R. M., Makimura Y., Toghill K., Nazar L. F., A multifunctional 3.5 V iron-based phosphate cathode for rechargeable batteries, *Nat. Mater.*, 2007, Vol. 6, P. 749–753.

21 Kosova N. V., Rezepova D. O., Podgornova O. A., Slobodyuk A. B., Petrov S. A., Avdeev M., A comparative study of structure, air sensitivity and electrochemistry of sodium iron pyrophosphates $Na_{2-x}Fe_{1+x/2}P_2O_7$ (x = 0; 0.44), *Electrochim. Acta*, 2017, Vol. 235, P. 42–55.

22 Kosova N. V., Rezepova D. O., Petrov S. A., Slobodyuk A. B., Electrochemical and chemical Na^+/Li^+ ion exchange in Na-based cathode materials: $Na_{1.56}Fe_{1.22}P_2O_7$ and $Na_3V_2(PO_4)_2F_3$, *J. Electrchem. Soc.*, 2016, Vol. 164, P. A6192–A6200.

23 Wood S. M., Eames C., Kendrick E., Islam M. S., Sodium ion diffusion and voltage trends in phosphates $Na_4M_3(PO_4)_2P_2O_7$ (M = Fe, Mn, Co, Ni) for possible high-rate cathodes, *J. Phys. Chem.* C., 2015, Vol. 119, No. 25, P. 15935–15941.

24 Kim H., Park I., Seo D.-H., Lee S., Kim S.-W., Kwon W. J., Park Y.-U., Kim C. S., Jeon S., Kang K., New iron-based mixed-polyanion cathodes for lithium and sodium rechargeable batteries: Combined first principles calculations and experimental study, *J. Am. Chem. Soc.*, 2012, Vol. 134, No. 25, P. 10369–10372.

25 Barker J., Saidi M. Y., Swoyer J. L., A sodium-ion cell based on the fluorophosphate compound $NaVPO_4F$, *Electrochem. Solid State Lett.*, 2003, Vol. 6, No. 1, P. A1–A4.

26 Serras P., Palomares V., Goni A., Gil de Muro I., Kubiak P., Lezama L., Rojo T., High voltage cathode materials for Na-ion batteries of general formula $Na_3V_2O_2(PO_4)_2F_{3-2x}$, *J. Mater. Chem.*, 2012, Vol. 22, No. 41, P. 22301–22308.

27 Bianchini M., Fauth F., Brisset N., Weill F., Suard E., Masquelier C., Croguennec L., A comprehensive investigation of the $Na_3V_2(PO_4)_2F_3$–$NaV_2(PO_4)_2F_3$ system by operando high resolution synchrotron X-ray diffraction, *Chem. Mater.*, 2015, Vol. 27, No. 8, P. 3009–3020.

28 Kosova N. V., Rezepova D. O., Mixed sodium-lithium vanadium fluorophosphates $Na_{3-x}Li_xV_2(PO_4)_2F_3$: The origin of the excellent high-rate performance, *J. Power Sources*, 2018, Vol. 408, P. 120–127.

29 Kosova N. V., Rezepova D. O., Effect of the La^{3+} modification on the electrochemical performance of $Na_3V_2(PO_4)_2F_3$, *Batteries*, 2018. Vol. 4, No. 3, Art. 32.